HOLOS
ISSN 1807 - 1600

NUMERICAL INVESTIGATION OF TURBULENCE CHARACTERISTICS AND SELF-SIMILARITY IN A HIGHLY AERATED STABLE HYDRAULIC JUMP USING LARGE EDDY SIMULATION

F.O. ANDRADE*, M.Y.M. TAKENOBU, M. MARQUES
Universidade Tecnológica Federal do Paraná
ORCID ID: https://orcid.org/0000-0003-4348-7966 *
fandrade@utfpr.edu.br*

Submitted October 23, 2023 - Accepted November 27, 2023

DOI: 10.15628/holos.2023.16313

ABSTRACT

This work presents a numerical study of a stable hydraulic jump at Froude number 4.25 and Reynolds number 1.15×10^5 inside a horizontal and rectangular channel with a length of 3.2 m, a width of 0.5 m and a height of 0.4 m using large eddy simulation (LES). Classical hydraulic jump characteristics are obtained, such as conjugate depths, jump length, void fraction and velocity profiles. The hydraulic jump maximum streamwise velocity decay and shear layer spreading rate are simulated and compared with experimental data. For these parameters, numerical results demonstrate that is possible to stablish an analogy with other shear flows, such as the horizontal plane wall jet. Profiles of streamwise and vertical components of mean velocity are simulated, and self-similarity is observed for cross-sections located at the recirculation region of the jump. Self-similarity is also observed in terms of turbulent fluctuations, insofar as LES simulations indicate a high level of turbulence in the recirculation region. The simulated root mean square of streamwise velocity fluctuations, u_{rms}, ranges from 0.5 to 0.7 of the maximum cross-sections velocity, whereas the root mean square of vertical component of velocity fluctuations, v_{rms}, stays around 0.5 of the maximum cross-sections velocitiy. All validation comparisons show good agreement with the selected experimental data of Kramer and Valero (2020) and Wang (2014), presenting average deviations always lesser than 5%.

KEYWORDS: Hydraulic jump, large eddy simulation, turbulence, self-similarity.

INVESTIGAÇÃO NUMÉRICA DAS CARACTERÍSTICAS DA TURBULÊNCIA E AUTO-SIMILARIDADE DE UM RESSALTO HIDRÁULICO ESTABILIZADO ALTAMENTE AERADO MEDIANTE USO DE SIMULAÇÃO DE GRANDES ESCALAS

RESUMO

Este trabalho apresenta um estudo numérico de um ressalto hidráulico estabilizado, a número de Froude 4.25 e número de Reynolds 1.15×10^5, posicionado em um canal horizontal de seção transversal retangular com comprimento de 3,2 m, largura de 0,5 m e altura 0,4 m, resolvido mediante aplicação do método de simulação de grandes escalas (LES). As características básicas do ressalto hidráulico são simuladas, como as profundidades conjugadas, comprimento do ressalto e perfis de velocidade e concentração de ar. O decaimento da velocidade máxima do ressalto hidráulico e a taxa de espalhamento da camada cisalhante são simulados e comparados com dados experimentais. Para esses parâmetros, os resultados numéricos demonstram que é possível estabelecer uma analogia com outros escoamentos cisalhantes, tais como o jato de parede plano. Perfis das componentes vertical e longitudinal da velocidade média são simulados, de modo que a autossimilaridade é observada para seções transversais localizadas na região de recirculação do ressalto. A autossimilaridade também é observada em termos de flutuações turbulentas, enquanto as simulações LES indicam um alto nível de turbulência na região de recirculação. A raiz quadrática média simulada da componente longitudinal da flutuação de velocidade, u_{rms}, varia de 0,5 a 0,7 da velocidade máxima das seções transversais e a raiz quadrática média simulada da componente vertical da flutuação de velocidade, v_{rms}, gira em torno de 0,5 da velocidade máxima das seções transversais. Todas as comparações de validação demonstraram boa concordância com os dados experimentais selecionados de Kramer and Valero (2020) and Wang (2014), apresentando desvios médios sempre menores que 5%.

Palavras chave: Ressalto hidráulico, simulação de grandes escalas, turbulência, auto-similaridade.

Este é um artigo publicado em acesso aberto sob uma licença Creative Commons.

HOLOS
ISSN 1807 - 1600

1 INTRODUCTION

Hydraulic jumps are commonly encountered in natural environments and oftentimes enforced in human-made facilities to generate mechanisms such as energy dissipation and mixing processes (Singh and Roy, 2023). The jumps are characterized by a rapid rise in free surface elevation at the transition from supercritical flow to subcritical flow, and are always accompanied by intense turbulence, energy dissipation and air entrainment (Witt et al., 2018). The strength of the hydraulic jumps can be measured by the inflow Froude number $Fr_1 = u_1/\sqrt{gd_1}$, where g is the acceleration of gravity, u_1 is the time and depth-averaged velocity and d_1 is the mean flow depth at the inflow section.

At the inflow section of the hydraulic jumps, a high velocity water jet impacts a slower portion of deeper water creating an inflection zone characterized by intense turbulence and air-water mixture (Kramer and Valero, 2020). This phenomenon is analogous to the horizontal wall jet, where the inflow boundary layer interacts with a developing shear layer of the jump and viscous forces start becoming relevant (Cavalcante et al., 2017). As in the horizontal wall jet, stable hydraulic jumps present a so-called developed region where self-similarity profiles in terms of mean velocity components and turbulence variables (i.e., mean longitudinal and transversal components of velocity, rms of velocity fluctuations) can be observed. A distinguish characteristic of hydraulic jumps is the substantial air entrainment coming from the surface fluctuations of the air-water interface, which is incorporated into the developing shear layer and carried downstream to the flow (Wudritch et al., 2022). A current research area of interest is concentrated on the measurement of turbulence characteristics using physical experiments or numerical simulations in the aerated regions of hydraulic jumps.

Most of the studies of turbulence characteristics in highly aerated hydraulic jumps available in literature have been performed experimentally using physical models. Chanson and Brattberg (2000) and Murzyn et al. (2005) investigated the distribution of air concentration, flow structure and bubble frequency in highly aerated hydraulic jumps for a wide range of Froude numbers using Prandtl-type pitot tube and phase-detection intrusive probes. Mossa (1999), Wang and Chanson (2015) and Montano (2018) studied the oscillating characteristics, cyclic mechanisms and water surface behavior of hydraulic jumps. Free-surface turbulent fluctuations were measured with electric hydrometers, acoustic displacement meters and more recently using Lidar technique. Wang and Murzyn (2017) and Wang and Chanson (2019) measured turbulent velocity and characteristic turbulent scales in highly aerated hydraulic jumps using arrays of wire gauges and phase-detection probes. Mossa and Tolve (1998) investigated a bubbly two-phase flow in a hydraulic jump using flow visualization technique. This pioneer study initiated a series of other experiments that performed turbulent velocity measurements based on imaging techniques, such as the works of Lin et al. (2012) and Bung and Valero (2016). Recent developments in imaging techniques for instantaneous velocity measurements in highly aerated hydraulic jumps have been demonstrated by the work of Kramer et al. (2019).

Numerical simulations have been used recently and provided researchers with a powerful tool to study the turbulent flow structures of hydraulic jumps. The direct numerical simulation (DNS) of Mortazavi et al. (2016) presented results for mean velocity fields, Reynolds stresses, turbulence production, turbulence dissipation, velocity spectra and air entrainment data. In

Este é um artigo publicado em acesso aberto sob uma licença Creative Commons.

HOLOS
ISSN 1807 - 1600

addition, this work reported complete statistics associated with bubble generation frequency. Jesudhas et al. (2016) performed a detached eddy simulation (DES) to study a submerged hydraulic jump. To validate the DES results, mean velocity and turbulence quantities including the Reynolds stresses were compared with available experimental data. Jesudhas et al. (2018) developed unsteady, improved, delayed, detached eddy simulation (IDDES) of an oscillating and unstable hydraulic jump at Froude numbers of 3.8 and 8.5, respectively. The different types of oscillations were analyzed by evaluating the instantaneous flow field. All flow features were accurately captured by the simulations and were presented by the authors with pertinent discussions. Mukha et al. (2022) performed a large eddy simulation (LES) of a classical hydraulic jump at inlet Froude number of 2. The computations were performed using the open-source software OpenFoam®, and the primary objective was to evaluate the influence of the modelling parameters on the predictive accuracy of the solutions. Takenobu et al. (2022) performed DES and also used a k-ω SST turbulence model to evaluate the open-source software OpenFoam® to represent adequately the mean waterline profile and air concentration recorded along a hydraulic jump at inlet Froude number of 7.5. Numerical results were compared against physical model data showing good agreement of final simulations.

Despite the recent developments, numerical studies involving the most relevant characteristics of turbulence in the aerated region of hydraulic jumps still need further advancements. With this aspect in mind, the objective of this study is to perform large eddy simulation (LES) of a highly aerated hydraulic jump at inflow Froude number $Fr_1 = 4.25$ to investigate: (a) classical hydraulic jump characteristics, such as conjugate depths, jump length and void fraction profiles, (b) hydraulic jump maximum longitudinal velocity decay, shear layer spreading rate and mean velocity profiles, (c) hydraulic jump self-similar free surface and mean velocity profiles, and (d) hydraulic jump self-similar properties and velocity fluctuation profiles. The results obtained by LES are compared against the experimental data measured in the recent works of Kramer and Valero (2020) and Wang (2014).

The remainder of this manuscript is organized as follows: section Mathematical formulation describes the LES conservation equations in the context of the finite volume based open-source software OpenFoam®. Section Available experimental data summarizes the experimental works employed for comparisons against the obtained numerical results. Section Numerical set-up describes the geometry and boundary conditions, numerical mesh, numerical solvers and discretization schemes characteristics. Section Results and discussions presents and discusses the obtained results for the hydraulic jump properties, mean velocities, turbulence characteristics, void fraction profiles, mean velocity profiles and self-similar properties, and section Conclusions and recommendations presents the conclusions and recommendations for future work.

2 MATHEMATICAL FORMULATION

In the LES framework, the hydraulic jump is described by the spatially filtered equations for mass and momentum conservation of a Newtonian and incompressible fluid. Using tensor notation in Cartesian coordinates, for i, j = 1, 2, 3, these equations can be written as:

Este é um artigo publicado em acesso aberto sob uma licença Creative Commons.

HOLOS
ISSN 1807 - 1600

$$\frac{\partial \bar{u}_i}{\partial x_i} = 0 \tag{1}$$

$$\frac{\partial \bar{\rho}\bar{u}_i}{\partial t} + \frac{\partial \bar{\rho}\bar{u}_i\bar{u}_j}{\partial x_j} = -\frac{\partial \bar{p}}{\partial x_i} + \frac{\partial \bar{\tau}_{ij}}{\partial x_j} + \frac{\partial \tau_{ij}^{SGS}}{\partial x_j} + \bar{\rho}\bar{g}_i \tag{2}$$

where ρ is the density, u_i and u_j are the velocity vector components, p is the pressure and g_i is the gravity. The upper bar indicates a spatially filtered property. In this work, the retained LES filter is an implicit box filter associated with the adopted numerical mesh. The filtered viscous stress tensor, $\bar{\tau}_{ij}$, is given by:

$$\tau_{ij} = \mu\left(\frac{\partial \bar{u}_i}{\partial x_j} + \frac{\partial \bar{u}_j}{\partial x_i}\right) \tag{3}$$

where μ is the kinematic viscosity (Pope, 2000).

The sub-grid scale viscous stress tensor $\tau_{ij}^{SGS} = -\bar{\rho}\left(\overline{u_i u_j} - \bar{u}_i\bar{u}_j\right)$ is modelled according to:

$$\tau_{ij}^{SGS} = \mu_{SGS}\left(\frac{\partial \bar{u}_i}{\partial x_j} + \frac{\partial \bar{u}_j}{\partial x_i}\right) \tag{4}$$

where μ_{SGS} is the sub-grid scale kinematic viscosity, obtained with the use of the Smagorinsky-Lilly model (Smagorinsky, 1963):

$$\mu_{SGS} = 2\bar{\rho}(C_S\Delta)^2\left|\bar{S}_{ij}\right| \tag{5}$$

where C_S is the Smagorinsky constant with typical values for channel flows around 0.10, $\Delta = \sqrt[3]{\Delta x \Delta y \Delta z}$ is the filter characteristic length scale associated with the Cartesian mesh local control volumes dimensions $\Delta x, \Delta y, \Delta z$ and $\bar{S}_{ij}$ is the resolved rate of strain tensor.

A conservation equation for an indicator function is used to represent the free surface and the indication of phase (air or water) in the context of a volume of fluid (VOF) method (Hirt and Nichols, 1981):

$$\frac{\partial \bar{\gamma}}{\partial t} + \frac{\partial \bar{\gamma}\bar{u}_i}{\partial x_i} = 0 \tag{6}$$

where γ is the interface-capturing volume fraction (Wang et al., 2015, Huang et al. 2019). Physical properties such as density and viscosity at any point are calculated as weighted averages based as follows:

$$\bar{\rho} = \bar{\rho}_w\bar{\gamma} + \bar{\rho}_a(1-\bar{\gamma}) \tag{7}$$

$$\bar{\mu} = \bar{\mu}_w\bar{\gamma} + \bar{\mu}_a(1-\bar{\gamma}) \tag{8}$$

where the subscripts *w* and *a* indicate water and air, respectively. Equations (1) to (8) are solved using the finite volume based open-source software OpenFoam® (Moukalled et al. 2016). Information about the numerical solution characteristics is provided on the numerical simulation set-up section.

Este é um artigo publicado em acesso aberto sob uma licença Creative Commons.

HOLOS
ISSN 1807 - 1600

3 AVAILABLE EXPERIMENTAL DATA

The numerical simulation performed in this work employs geometric and boundary conditions identical to the experimental setup of Kramer and Valero (2020). This recent experimental study also provides most of the data for the validation comparisons of the obtained final simulation results. Kramer and Valero (2020) performed experimental measurements of a highly aerated stable hydraulic jump at an inflow Froude number of 4.25, using novel intrusive phase-detection probe and imaging techniques. The experimental measurements included: characteristics of the hydraulic jump such as conjugate depths, jump length and surface profiles, air and bubble concentrations profiles, velocity decay, spreading rate and mean velocity components profiles, velocity fluctuations and Reynolds stresses profiles, turbulent integral length scales and turbulence spectra.

In addition, selected data from the experimental study of Wang (2014) are used for the validation comparisons against the obtained final simulation results. This PhD thesis presented a systematic study of classical hydraulic jumps based upon physical modelling. The study covered a wide range of inflow Froude numbers from 2.8 to 10, using intrusive and non-intrusive phase-detection probe techniques. The experimental measurements included quantities such as water level and pressure fluctuations, jump toe oscillations, air entrainment and void fraction profiles and instantaneous velocity fields.

4 NUMERICAL SIMULATION SET-UP

4.1 Geometry, boundary conditions and computational mesh

The numerical simulations are performed for water at standard temperature and pressure, with density $\rho = 998.2\ kg/m^3$ and kinematic viscosity $\mu = 1.0016 \times 10^{-3}\ Pa \cdot s$, flowing in a horizontal and rectangular channel with a length of $3.2\ m$, a width of $0.5\ m$ and a height of $0.4\ m$. A uniform discharge $q_1 = 0.057\ m^3/s \cdot m$ is used as inflow boundary condition leading to an inflow mean velocity of $3.16\ m/s$, with no velocity fluctuation applied at the inlet. At the outlet is adopted a fixed value velocity boundary condition of $0.47\ m/s$. The channel bottom, the left and right laterals walls are considered isothermal and no-slip walls, and the channel roughness effects are neglected to simulate the conditions of a smooth type of bed. The top plane is set to static atmospheric condition.

A preliminary computational mesh was developed by discretizing the geometry domain using polyhedrical control volumes in an orthogonal Cartesian coordinate system. Subsequently, a final refined mesh was constructed using the tool *blockMesh* available in the OpenFoam® package. In the transversal and longitudinal directions, the control volumes dimensions are uniform and equal to $\Delta z = 10\ mm$ and $\Delta x = 5mm$, respectively. In the vertical direction, the control volumes are extremely small in the region near the channel bottom, where the average wall y^+ is 44.69, gradually and slowly expanding towards the mean water surface level (region C), where dimensions are typically around $\Delta y \approx 0.5mm$. Above the mean water surface level, in the vertical direction towards the free atmosphere (region B), the control volumes expand to maximum sizes around $\Delta y \approx 2.5mm$. The total size of the mesh is 5,400,000 control volumes. The final solution was

Este é um artigo publicado em acesso aberto sob uma licença Creative Commons.

HOLOS
ISSN 1807 - 1600

obtained in 336 hours, running in an AMD-7452 cluster with 64 computational cores. Figure 1(a) shows a general mesh view and the applied boundary conditions, and figure 1(b) shows a detailed side view of the computational mesh.

The simulated hydraulic jump mean inflow depth is $d_1 = 0.042\ m$ and the mean depth at the end of the jump is $d_2 = 0.24m$, identical to the values obtained by Kramer and Valero (2020). The jump inflow time and depth averaged velocity is $u_1 = 2.73\ m/s$, leading to an inflow Froude number $Fr_1 = u_1/\sqrt{gd_1} = 4.25$. The Reynolds number is $Re = \rho u_1 d_1/\mu \approx 1.15 \times 10^5$. The jump toe location of the LES simulation is $x_1 = 0.4\ m$ from the upstream inflow boundary condition. The streamwise position along the computational domain is given by the following dimensionless parameter: $\chi = (x - x_1)/d_1$, where x is the streamwise coordinate, x_1 is the hydraulic jump toe average location and d_1 is the hydraulic jump inflow depth.

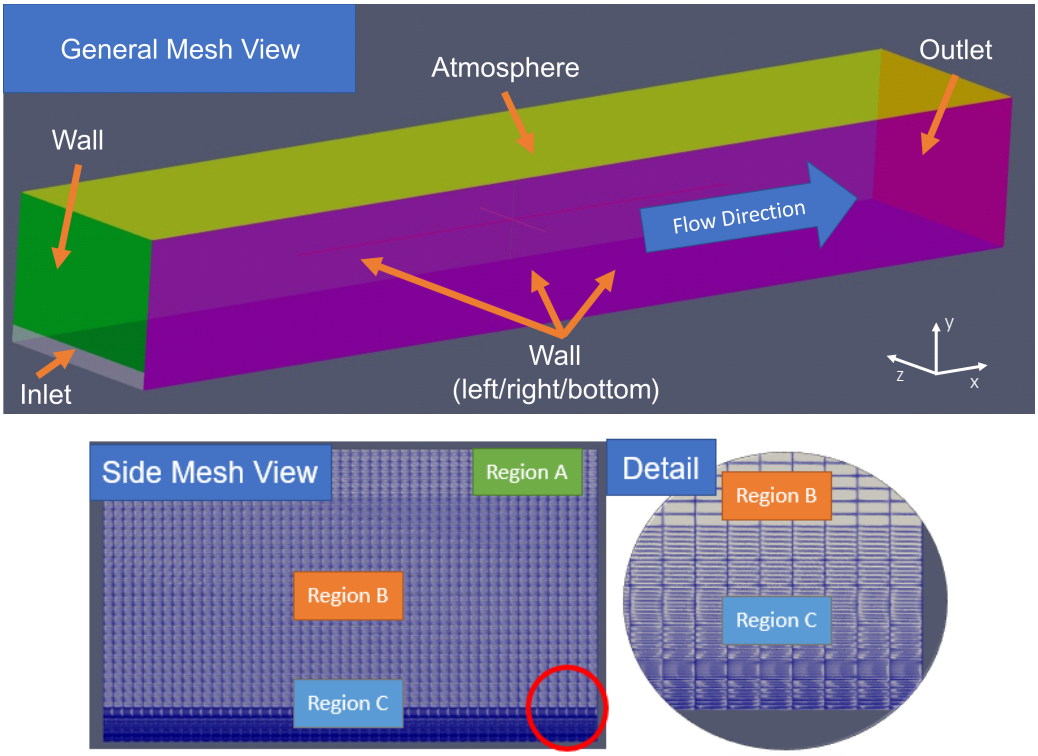

Figure 1: (a) General mesh view and boundary conditions, (b) Detail side view of the computational mesh.

4.2 Numerical solvers and discretization schemes

All simulations are performed using the software OpenFoam® version 8, a widely spread suite of solvers for continuum mechanics, based on the finite volume method (Patankar, 1980). The software package is designed to run natively in GNU/Linux systems, and the source code is open and written almost entirely in object-oriented C++. A central theme of the OpenFoam® design is that the solver applications, written using the OpenFoam® classes, have a syntax that closely resembles the partial differential equations being solved, a characteristic that eases the process of designing new solvers, implementing new models and equations.

In this work, the governing equations are solved on collocated and polyhedral mesh arrangements, considering turbulent flows of incompressible fluid in unsteady state. The temporal

Este é um artigo publicado em acesso aberto sob uma licença Creative Commons.

HOLOS ISSN 1807 - 1600

discretization is limited by the Courant–Friedrichs–Lewy (CFL) condition equals 0.5, leading to stable time steps varying approximately from 10^{-4} to 10^{-5} s. At each time step, the PIMPLE algorithm is used for pressure-velocity coupling. The matrices of the pressure equation are solved by a preconditioned conjugate gradient DIC (diagonal incomplete-Cholesky) method, whereas the momentum equations are solved by a Gauss Seidel smooth solver. All solver tolerances are set to 10^{-8}.

The spatial discretization schemes in OpenFoam® rely heavily on interpolation schemes to transform cell-based (centroid) quantities to cell faces (Barroso et al., 2015), since the mesh variable arrangement is collocated, in combination with Gauss Theorem to convert volume integrals to surface integrals. The equations gradients are solved using a cell limited Gauss linear scheme. The cell gradient is limited to preserve the monotonicity condition by ensuring that the face values obtained by extrapolating the cell value to the cell faces using the gradient are bounded by the neighboring cells minimum and maximum limits. The non-linear terms of momentum equations are discretized by a bounded second order upwind scheme and Laplacian terms are discretized by a Gauss linear corrected scheme.

4.3 Data statistics and validation criteria

The hydraulic jump achieved stability after 30 seconds of simulation, starting from initial conditions of the channel at rest. Once the hydraulic jump was completely stable, the statistics are collected for a frequency of 20 Hz during a period of 20 s, similarly as suggested by the work of Witt (2014). Results are extracted for a vertical plane located at the centerline of the computational domain (centerline position $2z/w = 0$) and next to the sidewall of the channel (sidewall position $2z/w = 0.96$), where z is the transversal coordinate and w is the width of the channel, for cross-sections located at χ = 3.6, 7.1, 10.7 and 14.3. In this work, numerical results are considered validated against the selected experimental data of Kramer and Valero (2020) and Wang (2014) if the deviations of the statistics are lesser than 10%. Figure 2 illustrates the positions of the dimensionless variable χ of the cross-sections used for comparisons against experimental data.

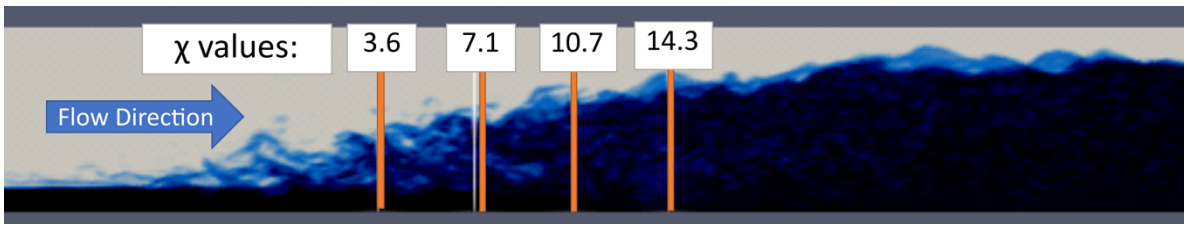

Figure 2: Positions of χ coordinates of the cross-sections for comparisons of LES results with experimental data.

5 RESULTS AND DISCUSSIONS

5.1 Conjugate depths, jump length and self-similar free surface profile

A well-known relationship of hydraulic jumps is the conjugate depths d_1, d_2, obtained by the application of the momentum equation under the assumption of negligible wall shear stress,

Este é um artigo publicado em acesso aberto sob uma licença Creative Commons.

HOLOS
ISSN 1807 - 1600

uniform velocities and hydrostatic pressure distributions at the beginning and end of the jump. The resulting equation was first derived by Bélanger (1840):

$$\frac{d_2}{d_1} = \frac{1}{2}\left(\sqrt{1 + 8Fr_1^2} - 1\right) \tag{9}$$

where the subscripts 1 and 2 refer to upstream and downstream positions of the jump. Figure 3(a) illustrates equation (9) plotted as a red line together with the result obtained by the LES simulation plotted as a black mark, the blue mark one-point measurement of Kramer and Valero (2020) and the experimental data of Wang (2014).

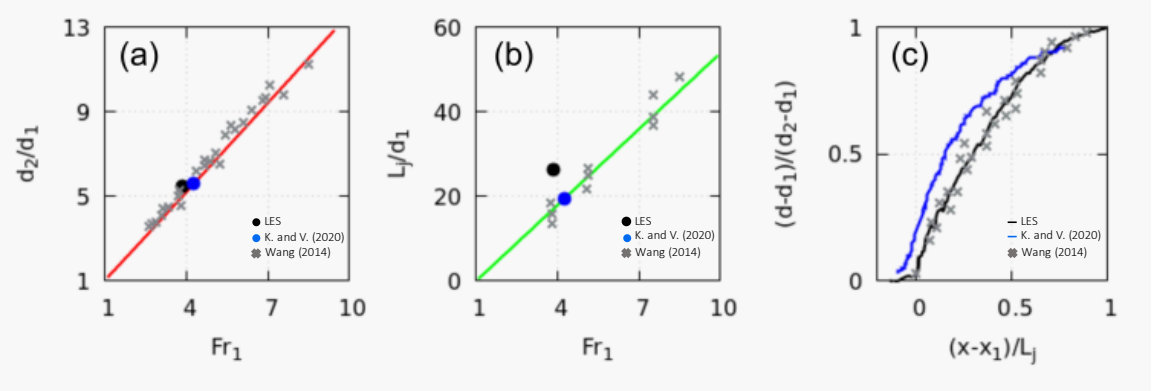

Figure 3: Basic hydraulic jump properties: (a) conjugate depth ratio d_2/d_1 as a function of inflow Froude number, (b) jump length ratio L_j/d_1 as a function of inflow Froude number, (c) self-similar free surface profile with d= free surface elevation.

Measurements of the hydraulic jump length usually present a degree of uncertainty. The jump length L_j can be defined as the distance between the jump toe and the location where the free surface becomes horizontal (Hager et al., 1990). Based on this definition, the resulting jump length of this LES simulation is $L_j = 1.16\ m$, whereas the Kramer and Valero (2020) measured $L_j = 0.82\ m$. Figure 3(b) shows that the equation $L_j/d_1 = c_1(Fr_1 - 1)$ holds, plotted as a green line, where $c_1 = 6$ is obtained by the adjustment of the points measured by Wang (2014). It can be observed that the LES simulated ratio L_j/d_1 is slightly higher than the experimental measurement.

A self-similar profile of the time-average hydraulic jump free water surface is given by:

$$\frac{d - d_1}{d_2 - d_1} = \left(\frac{x - x_1}{L_j}\right)^{c_2} \tag{10}$$

where d is the elevation of the free surface, d_1 and d_2 are the conjugate depths, L_j is the hydraulic jump length, $x_1 = 0.4\ m$ is the jump toe average location and x is the streamwise position. The exponent c_2 is equal to 0.537 based on the work of Wang (2014). Figure 3(c) illustrates the self-similar water surface profile. It is observed that the LES simulation profile represented by the black line is in perfect agreement with the experimental data of Wang (2014).

Este é um artigo publicado em acesso aberto sob uma licença Creative Commons.

HOLOS
ISSN 1807 - 1600

5.2 Void fraction distribution

Mean void fraction profiles, C, are computed next to the sidewall of the channel (at position $2z/w = 0.96$), where z is the transversal coordinate and w is the width of the channel. Four verticals are selected along the streamwise direction contemplating the two main regions of the hydraulic jump: the shear and recirculation regions. The four verticals are located at $\chi = 3.6, 7.1, 10.7$and 14.3. The mean void fraction profiles obtained for these cross-sections are plotted against the dimensionless depth y/d_1in Figures 4(a) to (d), respectively. It can be observed that for both shear and recirculation regions the LES simulation is able to capture the mean air-water interface behavior, showing a good agreement of mean void fraction distribution when compared to the measured data of Kramer and Valero (2020). The maximum average cross-section deviation is around 4.5%, therefore lesser than the 10% established as a benchmark criterion for the numerical results validation.

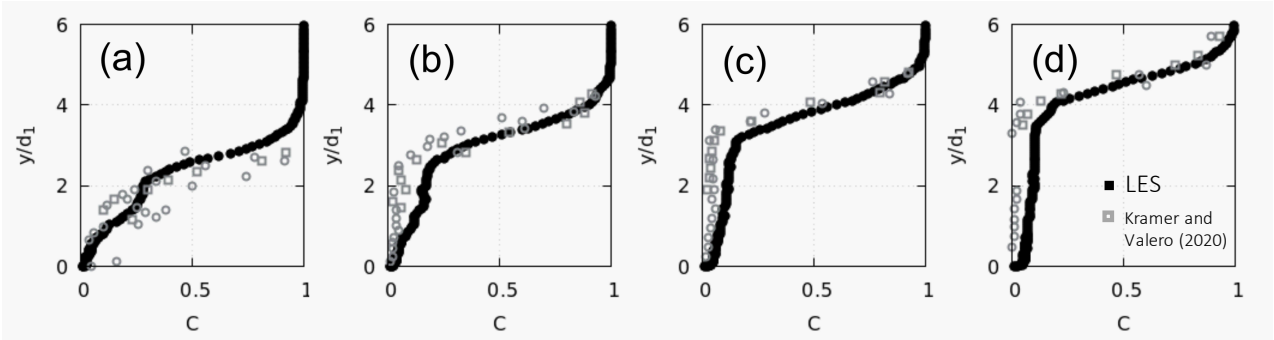

Figure 4: Void fraction distribution for cross-sections at: (a) $\chi = 3.6$, (b) $\chi = 7.1$, (c) $\chi = 10.7$, (d) $\chi = 14.3$.

5.3 Velocity decay, spreading rate and mean velocity profiles

There are two main characteristics of the impinging and roller region of the hydraulic jump: (1) velocity decay with increasing streamwise distance and (2) spreading rate of the hydraulic jump in the vertical direction. The velocity decay shows similar behavior of turbulent plane wall jets (Pope, 2000), where velocity declines proportionally to $u_{máx} \propto x^{-1/2}$, where $u_{máx}$ is the maximum streamwise cross-sectional velocity. Kramer and Valero (2020) obtained the following empirical relationship: $u_{máx}/u_1 = 1.9\chi^{-1/2}$. Figure 5(a) illustrates the streamwise velocity decay of the hydraulic jump at the centerline, comparing the simulation results in black marks with selected experimental data. It can be observed that LES simulated results positioned in the same range of the experimental data of Kramer and Valero (2020), Chanson (2009) and Chanson and Brettberg (2000).

Similar to turbulent plane jets, the shear layer of the hydraulic jump can be characterized by means of the spreading rate S, defined as the gradient of the hydraulics jump half-width $y_{1/2}$ in the streamwise direction, $S = dy_{1/2}/dx$, where the half-width fulfills the following condition: $\bar{u}(x, y_{1/2}) = 1/2\, u_{máx}$. Figure 5(b) illustrates the spreading rate of hydraulic jump in terms of the normalized half-width $y_{1/2}/d_1$. The LES simulation in black marks and the experimental data of Kramer and Valero (2020) lead to a perfect agreement, indicating that the hydraulic jump spread linearly at a rate of $S = 0.128$.

Este é um artigo publicado em acesso aberto sob uma licença Creative Commons.

HOLOS
ISSN 1807 - 1600

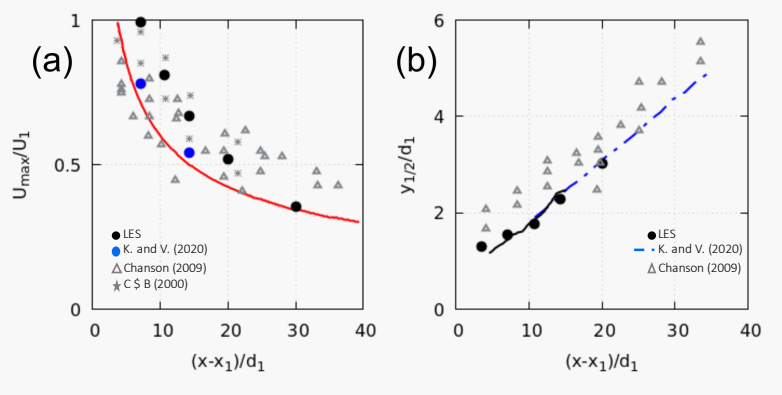

Figure 5: (a) Streamwise velocity decay at centerline, (b) normalized spreading rate at centerline - comparison with data from Kramer and Valero (2020), Chanson and Brattberg (2000) and Chanson (2009).

Mean velocity profiles are computed at the centerline and next to the sidewall of the channel. Figure 6 shows mean velocity profiles at four different positions from the hydraulic jump toe at $\chi = 3.6, 7.1, 10.7$ and 14.3. Figures 6(a) to (d) illustrates the development of the mean normalized streamwise component of the velocity in the jet region of the jump. It can be observed that the LES simulation predicted higher values when compared with the experimental measurements of Kramer and Valero (2020).

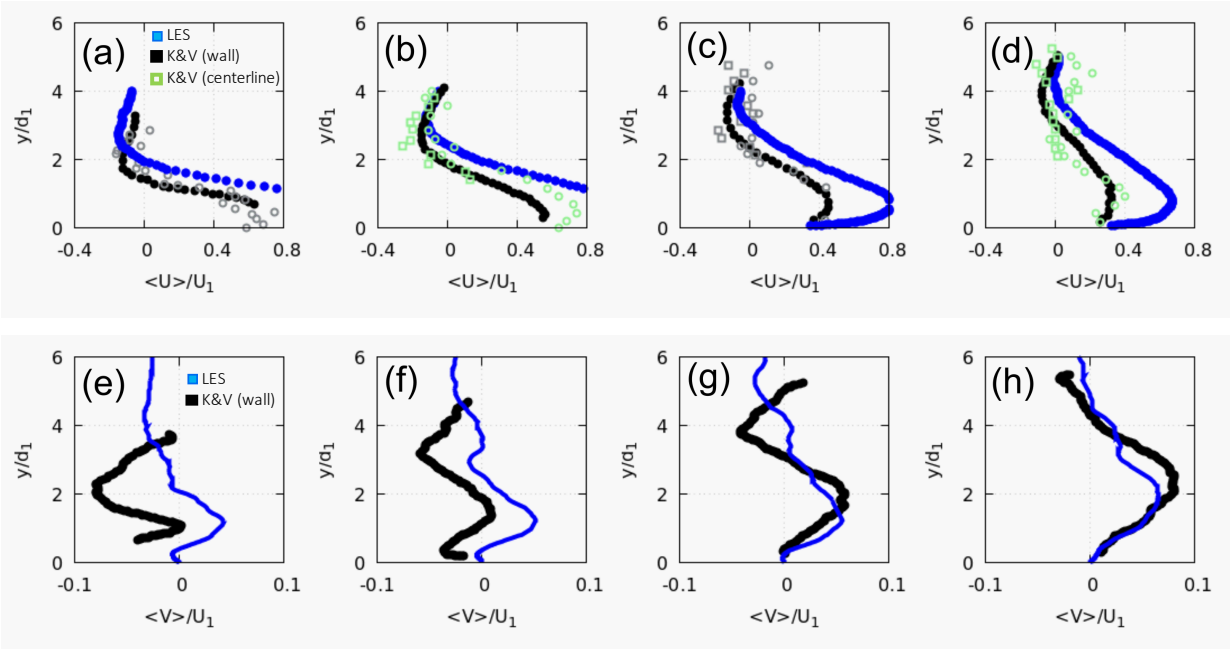

Figure 6: Mean velocity profiles. Streamwise component at positions: (a) $\chi = 3.6$, (b) $\chi = 7.1$, (c) $\chi = 10.7$, (d) $\chi = 14.3$, and transversal component at positions: (e) $\chi = 3.6$, (f) $\chi = 7.1$, (g) $\chi = 10.7$, (h) $\chi = 14.3$.

Figures 6(e) to (h) illustrates the development of the mean normalized vertical component of the velocity. The LES simulation captures the behavior of the vertical velocity for the cross-sections $\chi = 7.1$ to 14.3, whereas for the cross-section located in the shear region at $\chi = 3.6$, the

Este é um artigo publicado em acesso aberto sob uma licença Creative Commons.

HOLOS
ISSN 1807 - 1600

LES simulation did not provide the peak of negative vertical velocities as measured in the experiment of Kramer and Valero (2020).

5.4 Self-similar profiles of mean velocities and velocity fluctuations

The hydraulic jump demonstrates velocity self-similar behavior like other shear flows (i.e., plane turbulent jet, shear mixing layer) by using adequate dimensionless variables. Introducing the self-similar variables ξ and η in the vertical direction:

$$\xi = \frac{y}{y_{1/2}} \qquad \eta = \frac{y - y_{u_{máx}}}{y_{1/2} - y_{u_{máx}}} \tag{11}$$

with $y_{u_{máx}}$ being the elevation where $\bar{u} = u_{máx}$ and y the vertical direction, the velocity profiles can be expressed as a function of the self-similar variables:

$$f(\xi) = \frac{\bar{u}}{u_{máx}} \qquad g(\eta) = \frac{\bar{u} - u_{min}}{u_{máx} - u_{min}} \qquad h(\xi) = \frac{\bar{v} - v_{min}}{v_{máx} - v_{min}} \tag{12}$$

where $f(\xi)$ and $g(\eta)$ represent the streamwise velocity distribution and $h(\xi)$ the normal velocity distribution. Figure 7(a) shows the results of the LES simulation in blue marks for the self-similar distribution of streamwise velocity $f(\xi)$, compared with contours obtained by Kramer and Valero (2020) measured downstream of the impinging region for $\chi > 8$. It can be observed a quite good agreement between the LES simulation and measured data in representing the self-similar profile. The obtained LES results follow exactly the behavior of the empirical wall-jet equation $f(\xi) = 2.3(\xi)^{0.42}[1 - \mathrm{erf}(0.886\xi)]$ proposed by Verhoff (1963) and adapted by Lin et al. (2012), depicted by the solid red line. Figure 7(b) illustrates the self-similar streamwise velocity distribution $g(\eta)$ for the so-called upper region of the hydraulic jump, valid downstream of the impinging region for $\chi > 8$. The LES simulation in blue marks and the experimental data contours are in quite good agreement, both can be represented by the equation $g(\eta) = \exp(-\alpha\eta^2)$, where $\alpha \approx \ln 2$. Figure 7(c) shows the self-similar vertical velocity distribution $h(\xi)$. The LES simulation in blue marks indicates that $h(1) \approx 1$, hence $y_{v_{máx}} \approx y_{1/2}$. In addition, the vertical profile exhibits a *S*-shape profile that can be approximated by a Fourier series: $h(\xi) = \alpha_0 + \alpha_1 \cos(\xi\beta) + \alpha_2 \sin(\xi\beta)$, where $\alpha_0 = 0.5144$, $\alpha_1 = -0.2596$, $\alpha_2 = 0.3427$ and $\beta = 2.297$, indicated by the curve in red line. There is a quite good agreement between LES results and the contours of experimental data.

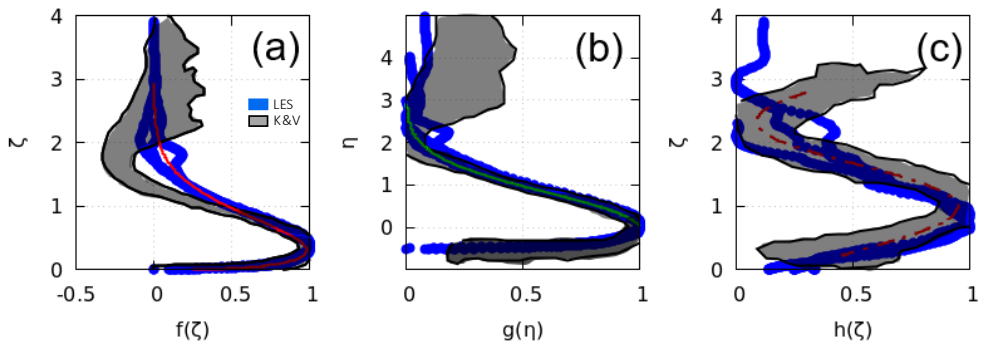

Figure 7: Self-similarity of mean velocity profiles downstream of impinging region for $\chi > 8$: (a) streamwise velocity with variables ξ and $f(\xi)$, (b) streamwise velocity with variables η and $g(\eta)$, (c) vertical velocity with variables ξ and $h(\xi)$.

Este é um artigo publicado em acesso aberto sob uma licença Creative Commons.

HOLOS
ISSN 1807 - 1600

The hydraulic jump is characterized by intense turbulent fluctuations, which can reach 50% or more of inflow velocities at the region next to the jump toe, exceeding the turbulence typically encountered in wall-jet flows. The streamwise component of the velocity fluctuation is the residual $u' = u - \bar{u}$, where u is the total velocity. The root mean square of velocity fluctuations is computed as $u_{rms} = \sqrt{\overline{u'^2}}$ and, similarly, for the vertical component of velocity fluctuation v_{rms}. It is also observed self-similarity in terms of velocity fluctuation components u_{rms} and v_{rms} downstream of the impinging region of the jump for $\chi > 8$. Figure 8(a) illustrates the self-similar distribution of normalized streamwise turbulent fluctuation $u_{rms}/u_{máx}$. It can be noticed that all profiles collapse into the same brush of curves showing self-similarity for the region $\chi > 8$ and a high level of turbulent fluctuations, where the u_{rms} ranges between 0.5 to 0.7 of the maximum velocity in the section. The LES simulation results show approximately the same range of turbulence fluctuations. Figure 8(b) illustrates the self-similar distribution of normalized vertical turbulent fluctuation $v_{rms}/u_{máx}$. The experimental data shows a high level of turbulent fluctuations for this component, ranging from $v_{rms}/u_{máx}$ approximately equal 0.35 to 0.65, whereas the LES simulation indicates level of $v_{rms}/u_{máx}$ in the range of 0.5.

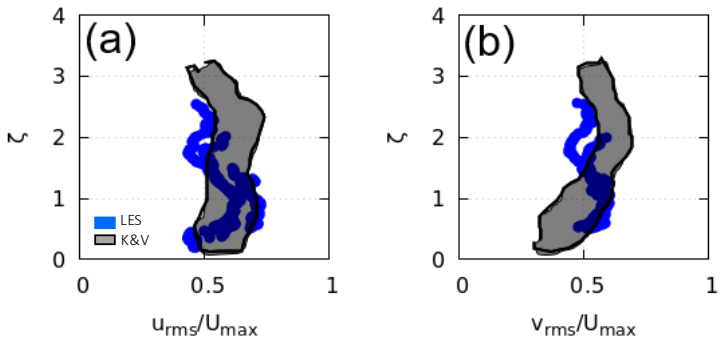

Figure 8: Self-similarity of turbulent velocity fluctuation profiles downstream of impinging region for $\chi > 8$: (a) streamwise component $u_{rms}/u_{máx}$ (b) vertical component $v_{rms}/u_{máx}$.

6 CONCLUSIONS AND RECOMMENDATIONS

This numerical study investigated a stable hydraulic jump at $Fr_1 = 4.25$ and $Re = 1.15 \times 10^5$ using large eddy simulation and open-source software OpenFoam®. The experimental study of Kramer and Valero (2020) provided the geometric and boundary conditions for the simulations, as well as the data for validation comparisons. Basic hydraulic jump properties, mean void fraction profiles, mean and fluctuating velocities were compared with selected data, in addition with the study of Wang (2014) and analytical data.

The LES simulation was able to calculate the basic hydraulic jump properties and also to predict the mean void fraction distribution in the shear region for the cross-section located at $\chi = 3.6$, and in the recirculation region at $\chi = 7.1, 10.7$ and 14.3, where deviations from the experimental data of Kramer and Valero (2020) were always lesser than 5%. LES results also showed that the hydraulic jump exhibits maximum velocity decay, spreading rate, and self-similarity in terms of mean and fluctuating velocity components comparable to other shear flows,

Este é um artigo publicado em acesso aberto sob uma licença Creative Commons.

HOLOS
ISSN 1807 - 1600

such as the plane wall-jets. The LES simulation indicated velocity decay equivalent to the measurements of Wang (2014), a spreading rate *S*=0.128 as in Kramer and Valero (2020) and was capable to accurately predict all self-similar mean velocity profiles. In terms of turbulent fluctuations, LES simulation demonstrated the existence of self-similar profiles for $\chi > 8$, and that the u_{rms} ranges approximately between 0.5 to 0.7 of the maximum streamwise velocity and the v_{rms} is around 0.5 of the maximum streamwise velocity for this region.

In the future, further numerical work will be developed as a second part of this research with the objective of exploring two different aspects: (1) the use of a more elaborated turbulence model, such as the dynamic Smagorinsky model, and (2) the investigation of other turbulence characteristics in the shear and recirculation regions of the hydraulic jump, such as the turbulence integral characteristic length and velocity scales, the Reynolds stress tensor components and the spectrum of turbulent kinetic energy. The knowledge of such properties of the hydraulic jump can be useful for applications involving mixture of composites and energy dissipation.

7 REFERENCES

Barroso, A. B., Bessa, J. A., Bezerra, C. A. D., Moraes, J. L., Alexandria, A. R. (2015). Análise do balancin da suspensão do protótipo fórmula por método dos elementos finitos. HOLOS.5, 170–181. https://doi.org/10.15628/holos.2015.2189

Bélanger, J. B. (1840). Notes sur Lhydraulique. Cole Royale des Ponts et Chausses, Champs-sur-Marne, France.

Bung, D., Valero, D. (2016). Optical flow estimation in aerated flows. *Journal of Hydraulic Research*, 54(5), 575-580. doi.org/10.1080/00221686.2016.1173600

Cavalcante, M. A., Chaves, S. G., Fagundes, F. P., Fagundes, K. R. G. (2017). Influência do tipo e da concentração de quebrados de géis no processo de fraturamento hidráulico. HOLOS. 1, 125–138. https://doi.org/10.15628/holos.2017.5196

Chanson, H. (2009). Advective diffusion of air bubbles in hydraulic jumps with large Froude numbers: An experimental study. Technical Report. School of Engineering, University of Queensland. Brisbane, Australia.

Chanson, H., Brattberg, T. (2000). Experimental study of the air-water shear flow in a hydraulic jump. *International Journal of Multiphase Flow*, 583-607.

Hager, W.H., Bremen, R., Kawagoshi, N. (1990). Classical hydraulic jump: length of roller. *J. Hydraul. Res*. 28, 591–608. doi/abs/10.1080/00221689009499048

Hirt, C. W., Nichols, B. D. (1981). Volume of Fluid (VOF) method for the dynamics of free boundaries. *Journal of Computational Physics*. 39, 201-225.

Huang, J., JiaJia, L., Politano, M., Li, R., Carrica, P. (2019). Modelling air entrainment downstream of spillways. *E-proceedings of the 38th IAHR World Congress*. Panama City, Panama. doi:10.3850/38WC092019-1317

Este é um artigo publicado em acesso aberto sob uma licença Creative Commons.

Jesudhas, V., Roussinova, V., Balachandar, R., Barron, R. (2016). Submerged Hydraulic Jump Study Using DES. *J. Hydraul. Eng*. 143(3): 04016091. doi/10.1061/%28ASCE%29HY.1943-7900.0001231

Jesudhas, V., Murzyn, F., Balachandar, R. (2018). IDDES evaluation of oscillating hydraulic jumps. *E3S Web of Conferences 40*. 05067. River Flow 2018. doi.org/10.1051/e3sconf/20184005067

Kramer, M., Valero, D. (2020). Turbulence and self-similarity in highly aerated shear flows: The stable hydraulic jump. *International Journal of Multiphase Flow*. 129. 103316. doi.org/10.1016/j.ijmultiphaseflow.2020.103316

Kramer, M., Valero, D., Chanson, H., Bung, D. (2019). Towards reliable turbulence estimations with phase-detection probes: an adaptive window cross-correlation technique. *Experiments in Fluids*. 60, 2-6. doi.org/10.1007/s00348-018-2650-9

Lin, C., Hsieh, S-C., Lin, I-J., Chang, K., Rajkumar, V. (2012). Flow property and self-similarity in steady hydraulic jumps. *Exp Fluids*. 53, 1591–1616. DOI 10.1007/s00348-012-1377-2

Montano, L., Li, R., Felder, S. (2018). Continuous measurements of time-varying free-surface profiles in aerated hydraulic jumps with a LIDAR. *Experimental Thermal and Fluid Science*. 93, 379-397. doi.org/10.1016/j.expthermflusci.2018.01.016

Mortazavi, M., Le Chenadec, V., Moin, P., Mani, A. (2016). Direct numerical simulation of a turbulent hydraulic jump: turbulence statistics and air entrainment. *Journal of Hydraulic Research*. 37, 541-558.

Mossa, M. (1999). On the oscillating characteristics of hydraulic jumps. *Journal of Hydraulic Research*. 37, 541-558. doi.org/10.1080/00221686.1999.9628267

Mossa, M., Tolve, U. (1998). Flow Visualization in Bubbly Two-Phase Hydraulic Jump. *Journal of Fluids Engineering*. 120, 160-165. DOI: 10.1115/1.2819641

Moukalled, F., Mangani, L., Darwish, M. (2016). The finite volume method in computational fluid dynamics: an advanced introduction with OpenFOAM and Matlab. *Springer International Publishing*, USA.

Mukha, T., Almeland, S. K., Bensow, R. E. (2022). Large-Eddy Simulation of a classical hydraulic jump: influence of modelling parameters on the predictive accuracy. *Fluids*. MPDI. 7-101. pp. 1-22. doi.org/10.3390/fluids7030101

Murzyn, F., Mouaze, D., Chaplin, J. R. (2005). Optical fibre probe measurements of bubbly flow in hydraulic jumps. *International Journal of Multiphase Flow*. 31, 141-154. doi:10.1016/j.ijmultiphaseflow.2004.09.004

Patankar, S. (1980). Numerical heat transfer and fluid flow. CRC Press. Boca Raton. USA.

Pope, S. B. (2000). Turbulent Flows. Cambridge University Press, Cambridge. https://doi.org/10.1017/CBO9780511840531

Smagorinsky, J. (1963). General circulation experiments with the primitive equations, I: the basic experiment. Monthly Weather Review. 91(3), 99-164.

Este é um artigo publicado em acesso aberto sob uma licença Creative Commons.

Singh, U. K., Roy, P. (2023). Energy dissipation in hydraulic jumps using triple screen layers. *Applied Water Science*. 13, 1-9. doi.org/10.1007/s13201-022-01824-y

Takenobu, M. Y. M., Dettmer, P. H. C., Ovelar, C. O. S., Souza, F. F., Andriolo, M. V., Giordani, S., Aver, C. S. (2022). Modelagem computacional de um ressalto hidráulico utilizando OpenFOAM. *Congresso Latino-americano de Hidráulica*. *Anais de mecânicas dos fluidos e hidráulica fundamental*. 78-86.

Verhoff, A. (1963). The two-dimensional turbulent wall jet with and without and external free stream. Technical report. Princeton. USA.

Wang, H. (2014). Turbulence and Air Entrainment in Hydraulic Jumps. PhD Thesis. School of Civil Engineering. The University of Queensland. Australia.

Wang, H., Chanson, H. (2015). Experimental study of turbulent fluctuations in hydraulic jumps. *J. Hydraul. Eng*. 141(7) 04015010. DOI: 10.1061/(ASCE)HY.1943-7900.0001010

Wang, H., Chanson, H. (2019). Characterization of transverse turbulent motion in quasi-two-dimensional aerated flow: Application of four-point air-water flow measurements in hydraulic jump. *Experimental Thermal and Fluid Science*. 100, 222-232. doi.org/10.1016/j.expthermflusci.2018.09.004

Wang, H., Murzyn, F. (2017). Experimental assessment of characteristic turbulent scales in two-phase flow of hydraulic jump: from bottom to free surface. *Environ Fluid Mech*.17, 7-25. DOI 10.1007/s10652-016-9451-6

Witt, A. M. (2014). Analytical and numerical investigation of an air entraining hydraulic jump. PhD Thesis. University of Minnesota.

Wang, Y., Politano, M., Laughery, R., Weber, L. (2015). Model development in OpenFOAM to predict spillway jet regimes. *Journal of Applied Water Engineering and Research*. 1-15, doi.org/10.1080/23249676.2015.1025442

Witt, A., Gulliver, J. S., Shen, L. (2018). Numerical investigation of vorticity and bubble clustering in an air entraining hydraulic jump. *Computers and Fluids*. 172, 162-180. doi.org/10.1016/j.compfluid.2018.06.019

Wudritch, D., Shi, R., Chanson, H. (2022). Hydraulic jumps with low inflow Froude numbers: air–water surface patterns and transverse distributions of two-phase flow properties. *Environmental Fluid Mechanics*. 22, 789-818. doi.org/10.1007/s10652-022-09854-5

HOW TO CITE THIS ARTICLE

Oliveira de Andrade, F., Yudi Minoda Takenobu, M., & Marques, M. NUMERICAL INVESTIGATION OF TURBULENCE CHARACTERISTICS AND SELF-SIMILARITY IN A HIGHLY AERATED STABLE HYDRAULIC JUMP USING LARGE EDDY SIMULATION. *HOLOS*, *5*(39). Recuperado de https://www2.ifrn.edu.br/ojs/index.php/HOLOS/article/view/16313

Este é um artigo publicado em acesso aberto sob uma licença Creative Commons.

HOLOS
ISSN 1807 - 1600

ABOUT THE AUTHORS

F. O. ANDRADE
Possui graduação em engenharia civil pela Universidade Federal do Paraná (1998), mestrado em engenharia civil e ambiental pela Universidade de Iowa, Estados Unidos (2000), doutorado em engenharia mecânica pela Pontifícia Universidade Católica do Rio de Janeiro (2009) e doutorado em mecânica dos fluidos pela Universidade de Poitiers, França (2009). É professor do curso de engenharia civil e do curso de engenharia sanitária e ambiental da Universidade Tecnológica Federal do Paraná desde 2013, onde leciona as disciplinas de mecânica dos fluidos e transferência de calor, hidráulica e hidrologia. É professor no Programa de Pós-graduação em Engenharia de Recursos Hídricos e Ambiental da Universidade Federal do Paraná desde 2012, onde leciona as disciplinas de mecânica dos fluidos ambiental I e II.
E-mail: fandrade@utfpr.edu.br
ORCID ID: https://orcid.org/0000-0003-4348-7966

M. Y. M. TAKENOBU
Possui graduação em engenharia civil pela Universidade Federal do Paraná e atualmente é mestrando em engenharia de recursos hídricos pelo Programa de Pós-Graduação em Engenharia de Recursos Hídricos e Ambiental da Universidade Federal do Paraná (PPGERHA-UFPR). É engenheiro pesquisador do Instituto LACTEC.
E-mail: marcelo.takenobu@lactec.com.br
ORCID ID: https://orcid.org/0009-0008-9720-1373

M. MARQUES
Possui graduação em engenharia civil pela Universidade estadual de Maringá e doutorado em engenharia de Recursos Hídricos pelo Programa de Pós-Graduação em Engenharia de Recursos Hídricos e Ambiental da Universidade Federal do Paraná (PPGERHA-UFPR). Atualmente é professor de Hidráulica e Mecânica dos Fluidos da Universidade Estadual de Maringá no Campus Umuarama.
E-mail: mmarques@uem.br
ORCID ID: https://orcid.org/0000-0001-5451-5323

Editor: Francinaide de Lima Silva Nascimento
***Ad Hoc* Reviewer:** Hemerson Pinheiro e Marco Antonio Jacomazzi

Submitted October 23, 2023
Accepted November 27, 2023
Published December 18, 2023

Este é um artigo publicado em acesso aberto sob uma licença Creative Commons.